Operation and Control of a Hybrid Microgrid Containing Unbalanced and Nonlinear Loads

Farhad Shahnia, Ritwik Majumder, Arindam Ghosh, Gerard Ledwich and Firuz Zare

School of Engineering, Queensland University of Technology, Brisbane, Australia

Abstract— This paper shows how the power quality can be improved in a microgrid that is supplying a nonlinear and unbalanced load. The microgrid contains a hybrid combination of inertial and converter interfaced distributed generation units where a decentralized power sharing algorithm is used to control its power management. One of the distributed generators in the microgrid is used as a power quality compensator for the unbalanced and harmonic load. The current reference generation for power quality improvement takes into account the active and reactive power to be supplied by the micro source which is connected to the compensator. Depending on the power requirement of the nonlinear load, the proposed control scheme can change modes of operation without any external communication interfaces. The compensator can operate in two modes depending on the entire power demand of the unbalanced nonlinear load. The proposed control scheme can even compensate system unbalance caused by the single-phase micro sources and load changes. The efficacy of the proposed power quality improvement control and method in such a microgrid is validated through extensive simulation studies using PSCAD/EMTDC software with detailed dynamic models of the micro sources and power electronic converters.

Index Terms: Microgrid, Power Quality, Power Sharing, Micro Source, Nonlinear Load

1. INTRODUCTION

The ever increasing energy demand, along with the necessity of cost reduction and higher reliability requirements, are driving the modern power systems towards distributed generation (DG) as an alternative to the expansion of the current energy distribution systems [1]. In particular, small DG systems, typically with power levels ranging from 1 kW to 10 MW, located near the loads are gaining popularity due to their higher operating efficiencies. Fuel cells (FC), Photovoltaic cells (PV), Batteries, micro turbines, etc. are nowadays the most available DGs for generation of power mostly in peak times or in rural areas [2].

A diesel generator set (genset) consists of an internal combustion engine, exciter and a synchronous generator coupled on the same shaft. Such systems are widely used as backup or emergency power in commercial as well as industrial installations. Diesel gensets are also extensively used in remote locations where no utility supply exists [3]. Over the last few decades, there is a growing interest in FC system for power generation and it has been identified as a suitable solution for distributed generation [4]. Other than FC, the use of new efficient PVs has emerged as an alternative measure of renewable green power, energy conservation and demand side management [5].

Microgrids are systems with clusters of loads and micro sources. To deliver high quality and reliable power, the microgrid should appear as a single controllable unit that responds to changes in the system [6]. The high penetration of DGs, along with different types of loads, always raises concern about coordinated control and power quality issues. In microgrid, parallel DGs are controlled to deliver the desired active and reactive power to the system while local signals are used as feedback to control the converters. The power sharing among the DGs can be achieved by controlling two independent quantities– frequency and fundamental voltage magnitude [7-9].

General introduction on microgrid basics, including the architecture, protection and power management is given in [10]. A review of on going research projects on microgrid in US, Canada, Europe and Japan is presented in [11]. Different Power management strategies and controlling algorithms for a microgrid is proposed in [12]. References [13-16] have evaluated the feasibility for the operation of the microgrids during islanding and synchronisation. An algorithm was proposed in [17] and used for evaluation of dynamic analysis for grid connected and autonomous modes of the microgrid. In [18], it is shown that a proper control method of distributed resources can improve the power quality of the network. There are still many issues which are needed to be addressed to improve the power quality in a microgrid.

The power quality issues are important as the power electronic converters increase the harmonic levels in the network voltage and current. Unbalance loads can cause the current and hence the voltage of the network suffering from high values of negative sequence which can be a problem for all induction motor loads in the network. Nonlinear loads (NL) can increase the harmonic level of the network current and voltage, which will increase the loss and reduce the efficiency of the network [19-20]. On the other hand, a power electronic converter can mitigate harmonic and unbalanced load or source problems. In [20] a series-shunt compensator is added in microgrid to achieve an enhancement of both the quality of power within the microgrid and the utility grid. The compensator has a series element as well as a shunt element. The series element can compen-

Corresponding Author: ritwik.majumder@student.qut.edu.au

sate for the unwanted positive, negative, and zero sequence voltage during any utility grid voltage unbalance, while the shunt element is controlled to ensure balanced voltages within the microgrid and to regulate power sharing among the parallel-connected DG systems. The proposed method in [20] requires adding other converters, while the same power quality improvement objectives can be achieved by one of the existing converters in the microgrid as proposed and validated in this paper.

To investigate the operation of all the micro sources together, a microgrid test bed is planned to be established at Queensland University of Technology (QUT) where issues such as decentralized power sharing and enhanced power quality operation will be tested. The QUT conceptual system with the technical parameters of its micro sources will be used as the test system in this paper.

One of the main contributions of the paper is the formulation of the compensator reference both when the compensator is able to supply the entire nonlinear load and when it is not. Furthermore, the compensator not only compensates the nonlinearity in the system but also shares power with other sources in the microgrid. In addition, inclusion of dynamics of the micro sources validates the feasibility of power sharing amongst inertial and converter interfaced micro sources. Finally, the paper demonstrates how to compensate the single-phase residential loads that maybe connected to the microgrid.

In this paper, the power quality enhanced decentralized power sharing is investigated in an autonomous microgrid with inertial and converter interfaced micro sources. To investigate the system response with the dynamics of the DGs, the micro sources and all the power electronic interfaces are modelled in detail. One of the converter interfaced sources is used as the compensator of the nonlinear and unbalanced load while the other DGs share the system load proportional to their rating based on droop control. The compensating DG can work in different operational modes depending on the power requirement of the local nonlinear load from just supplying a part of the nonlinear load to sharing some power of the microgrid loads while functioning as a compensator. Also, the compensation principle is tested on a low voltage residential distribution network that is connected to the microgrid. It is assumed that this low voltage network supplies single-phase residential loads with few installed PVs, connected at different phases. The efficacy of the proposed control scheme is validated through PSCAD/EMTDC simulation studies.

2. MICROGRID STRUCTURE

The schematic diagram of the microgrid system under consideration is shown in Fig. 1. There are four DGs as shown; one of them is an inertial DG (diesel generator) while others are converter interfaced DGs (PV, FC and battery). There are four resistive heater loads and six induction motor loads. A nonlinear load, which is a combination of unbalance and harmonic load, is also connected to BUS 5 in the microgrid. The FC will be used as the compensating DG for power quality improvement in this structure since it is the closest amongst all the converter interfaced DGs to the nonlinear load and connected to the same bus. If the nonlinear load was connected to BUS 3 or 4, the PV or battery should be used as the compensating DG. A discussion on the compensator location and the criteria for its placement is given in Appendix A. The parameters of the microgrid, loads, DGs and their converters are given in the Appendix B. In this paper, the autonomous operation mode of the microgrid is studied.

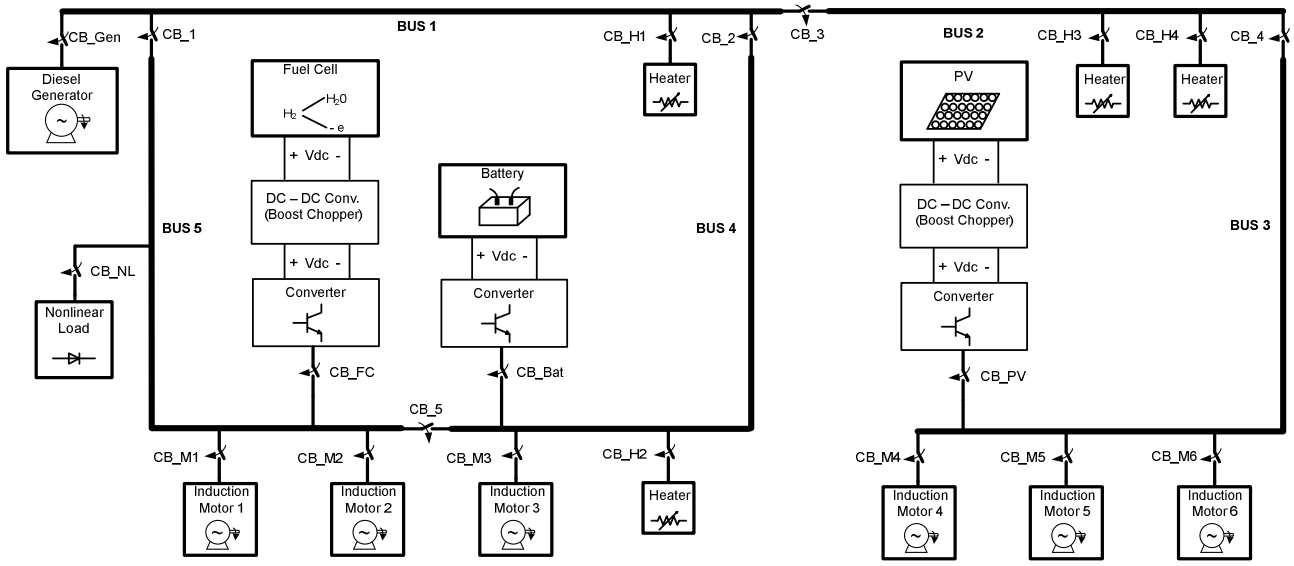

Fig.1 Schematic diagram of the microgrid structure under consideration.

3. DROOP CONTROL METHOD IN MICROGRID

In this section, the power sharing method in the microgrid is discussed. The decentralized power sharing among the DGs is achieved by the use of conventional droop control [7-8] as

$$\begin{aligned} \omega &= \omega_s - m\left(P - P_{rated}\right) \\ V &= V^* - n\left(Q - Q_{rated}\right) \end{aligned} \tag{1}$$

where m and n are the droop coefficients taken proportional to rated power of DGs for power sharing among them, ω_s is the synchronous frequency, V^* is the nominal magnitude of the network voltage, V is the magnitude of the converter output voltage and ω is its frequency, while P and Q respectively denote the active and reactive power supplied by the converter, (The suffix *rated* represents the rated power). Thus the frequency and the voltage are being controlled respectively by the active and reactive power output of the DG sources. Therefore, according to [7-8], the principles of decentralized power sharing in a microgrid is based on keeping proportional power output based on the rating of the DGs and power sharing amongst DGs are given by

$$\begin{aligned} &\frac{P_1}{P_2} \approx \frac{m_2}{m_1} = \frac{P_{1rated}}{P_{2rated}} \quad , \quad \frac{P_1}{P_3} \approx \frac{m_3}{m_1} = \frac{P_{1rated}}{P_{3rated}} \quad , \quad \ldots \\ &\frac{Q_1}{Q_2} \approx \frac{n_2}{n_1} = \frac{Q_{1rated}}{Q_{2rated}} \quad , \quad \frac{Q_1}{Q_3} \approx \frac{n_3}{n_1} = \frac{Q_{1rated}}{Q_{3rated}} \quad , \quad \ldots \end{aligned} \tag{2}$$

where the number suffixes show the number of each DG in the microgrid. The reference angle for the non inertial DGs (genset) is derived from the reference frequency.

4. COMPENSATOR CONTROL

In this section, the compensator control method and reference generation for the compensating DG is presented. As mentioned before, depending on the power requirement of the local nonlinear load, the compensating DG (FC) can work in different operational modes. If the required power of the local nonlinear load is less than the power rating of the FC, the compensating DG supplies the local nonlinear load totally and then the rest of the power is fed to the to the microgrid (Mode I). While the power requirement of the local nonlinear load is more than the rating of the compensating DG, the extra power requirement is supplied from the other micro sources in the microgrid (Mode II). In both of the modes, the other three micro sources (genset, PV and battery) always share the power proportional to their rating through the droop control. The most important aim of the compensator is supplying a current to the point of common coupling (PCC) that balances the voltage v_p at PCC and therefore, a balanced and non harmonic current will be drawn or injected to the microgrid. The schematic structure of the compensator is shown in Fig. 2.

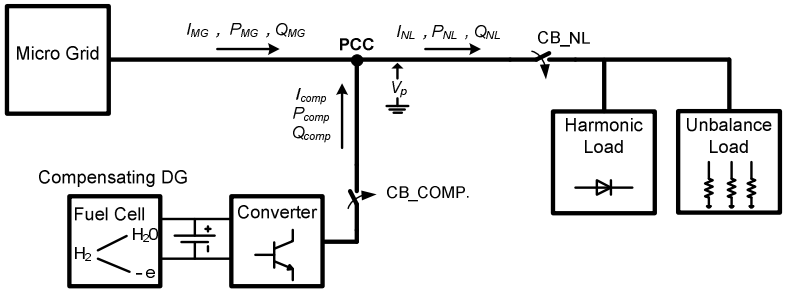

Fig. 2. Schematic diagram of the compensator.

As has been shown in [21], the compensator current that needs to be supplied to the microgrid is given by

$$\begin{bmatrix} i_{comp.a} \\ i_{comp.b} \\ i_{comp.c} \end{bmatrix} = \begin{bmatrix} i_{NLa} \\ i_{NLb} \\ i_{NLc} \end{bmatrix} - \frac{1}{K} \begin{bmatrix} 3P_{MG}v_{pa} + \sqrt{3}Q_{MG}\left(v_{pb} - v_{pc}\right) \\ 3P_{MG}v_{pb} + \sqrt{3}Q_{MG}\left(v_{pc} - v_{pa}\right) \\ 3P_{MG}v_{pc} + \sqrt{3}Q_{MG}\left(v_{pa} - v_{pb}\right) \end{bmatrix} \tag{3}$$

where, as shown in Fig. 2, P_{MG} and Q_{MG} respectively are the active and reactive power drawn/supplied to the microgrid, i_{comp} is the compensator current, i_{NL} is the nonlinear load current, v_p is the PCC voltage and the three phases are denoted by the subscripts a, b and c and $K = v_{pa}^2 + v_{pb}^2 + v_{pc}^2$. From (3), we derive the current injection requirements for the two modes, which are discussed below.

4.1. Mode I

In this mode, it is assumed that the power demand of the nonlinear load is less than the rated power of the compensating DG. Therefore, the compensator supplies the whole demand of the nonlinear load and a part of the power requirement of the other loads in the microgrid. Therefore, it is expected that the microgrid current $I_{MG,}$ and active and reactive power P_{MG} and Q_{MG} shown in Fig. 2 are negative. So, the power that can be injected by the compensator to the microgrid will be

$$\begin{aligned} -P_{MG} &= P_{comp,rated} - P_{NL} \\ -Q_{MG} &= Q_{comp,rated} - Q_{NL} \end{aligned} \tag{4}$$

where $P_{comp,rated}$ and $Q_{comp,rated}$ respectively are the rated active and reactive power output of the FC, which are calculated based on the maximum current that can be supplied by the FC. We can then modify (3) to get the following reference currents

$$\begin{bmatrix} i_{comp.a} \\ i_{comp.b} \\ i_{comp.c} \end{bmatrix} = \begin{bmatrix} i_{NLa} \\ i_{NLb} \\ i_{NLc} \end{bmatrix} + \frac{1}{K} \begin{bmatrix} 3\left(P_{comp._{rated}} - P_{NL}\right)\times v_{pa} + \sqrt{3}\left(Q_{comp._{rated}} - Q_{NL}\right)\times\left(v_{pb} - v_{pc}\right) \\ 3\left(P_{comp._{rated}} - P_{NL}\right)\times v_{pb} + \sqrt{3}\left(Q_{comp._{rated}} - Q_{NL}\right)\times\left(v_{pc} - v_{pa}\right) \\ 3\left(P_{comp._{rated}} - P_{NL}\right)\times v_{pc} + \sqrt{3}\left(Q_{comp._{rated}} - Q_{NL}\right)\times\left(v_{pa} - v_{pb}\right) \end{bmatrix} \tag{5}$$

Eq. (5) remains valid as long as the nonlinear load power demand is less than the rated power of the compensating DG. In case the power requirement is increased to more than the compensator rating, the control scheme will change the operation to Mode II.

4.2. Mode II

In Mode II, it is assumed that the power demand of the local nonlinear load is more than the rated power of the compensating DG. The compensating DG can supply a part of the total demand of the nonlinear load ensuring power quality improvement, while the rest of the required power is supplied from the microgrid side. This power is shared among the other three micro sources with all other microgrid loads based on droop control as described in Section 3.

It is expected that $I_{MG,}$ P_{MG} and Q_{MG} are all positive with respect to the sign convention direction shown in Fig. 2. The amount of the nonlinear load power supplied by the compensator can be a fixed fraction of the whole power or equal to the rating of the compensating DG. Therefore, we have:

$$\begin{aligned} P_{MG} &= P_{Lav} - P_{comp.} = P_{Lav} - \lambda_P.P_{Lav} = P_{Lav}\left(1-\lambda_P\right) \\ Q_{MG} &= Q_{Lav} - Q_{comp.} = Q_{Lav} - \lambda_Q.Q_{Lav} = Q_{Lav}\left(1-\lambda_Q\right) \end{aligned} \tag{6}$$

where P_{Lav} and Q_{Lav} are respectively the average active and reactive power demand of nonlinear load and λ_P ($0 < \lambda_P < 1$) and λ_Q ($0 < \lambda_Q < 1$) are respectively fractions of the active and reactive power supplied by compensating DG to the nonlinear load. We can substitute (6) in (3) to obtain

$$\begin{bmatrix} i_{comp.a} \\ i_{comp.b} \\ i_{comp.c} \end{bmatrix} = \begin{bmatrix} i_{NLa} \\ i_{NLb} \\ i_{NLc} \end{bmatrix} - \frac{1}{K} \begin{bmatrix} 3P_{Lav}\left(1-\lambda_P\right)\times v_{pa} + \sqrt{3}Q_{Lav}\left(1-\lambda_Q\right)\times\left(v_{pb} - v_{pc}\right) \\ 3P_{Lav}\left(1-\lambda_P\right)\times v_{pb} + \sqrt{3}Q_{Lav}\left(1-\lambda_Q\right)\times\left(v_{pc} - v_{pa}\right) \\ 3P_{Lav}\left(1-\lambda_P\right)\times v_{pc} + \sqrt{3}Q_{Lav}\left(1-\lambda_Q\right)\times\left(v_{pa} - v_{pb}\right) \end{bmatrix} \tag{7}$$

5. CONVERTER STRUCTURE

The converter interfaced micro sources like PV, FC and battery are connected to the microgrid through voltage source converters (VSC) as shown in Fig. 1. Output DC voltages of PV and FC are regulated by DC-DC choppers to control the power flow. The VSC structure and control of the micro sources including the compensator is discussed in this section.

5.1. Compensator VSC structure

The compensating DG has a VSC structure consisted of three single-phase H-bridges using IGBTs as shown in Fig. 3. The outputs of each H-bridge are connected to single-phase transformers and the three transformers are star connected. The VSC is utilizing a closed-loop optimal robust controller based on state feedback. The resistance R_f represents the switching and transformer losses, while the inductance L_f represents the leakage reactance of the transformers and the filter capacitor C_f is connected to the output of the transformers to bypass the switching harmonics.

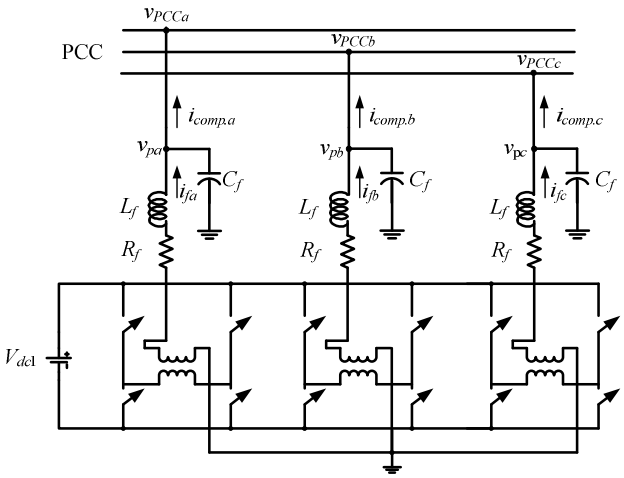

Fig. 3. Schematic diagram of the VSC for compensating DG.

The single-phase equivalent circuit of the VSC is shown in Fig. 4. The rest of the network is represented by voltage source V_{eq} and equivalent resistance (R_{eq}) and inductance (L_{eq}) as shown in the figure. In this figure, $u \cdot V_{dc1}$ represents the converter output voltage, where u is the switching function that can take on ±1 value depending on which pair of the IGBTs is turned on. The main aim of the converter control is to generate u.

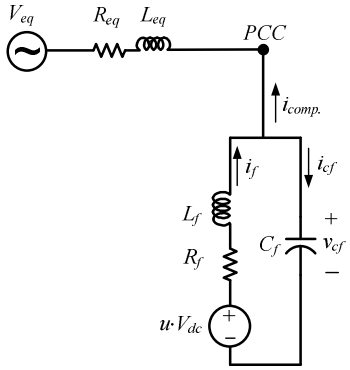

Fig. 4. Single-phase equivalent circuit of VSC for compensating DG at PCC.

Let the state vector be defined by

$$x^T = \begin{bmatrix} v_{cf} & i_{cf} & i_{comp} \end{bmatrix} \tag{8}$$

From the circuit of Fig. 4, state space description of the system can be given as

$$\dot{x} = A\,x + B_1\,u_c + B_2\,V_{eq} \tag{9}$$

where u_c is the continuous time version of switching function u. The discrete-time equivalent of (9) is

$$x(k+1) = Fx(k) + G_1 u_c(k) + G_2 v_{eq}(k) \tag{10}$$

Based on this model and a suitable feedback control law, $u_c(k)$ is computed. In this paper, capacitor reference voltage generation is based on measurement of the PCC voltage and calculating the fundamental voltage amplitude and angle. Later, the PCC voltage is fixed at the calculated voltage amplitude and angle by appropriate switching of IGBTs. The switching control laws are given by

$$u_c(k) = -K\left[x(k) - x_{ref}(k)\right] \tag{11}$$

where k is a gain matrix and x_{ref} is the reference vector. The gain matrix in this paper was obtained by LQR based on optimal control which ensures the desired results of the system while the variations of system load and source parameters are within acceptable limits of reality. From $u_c(k)$, the switching function is the generated based on an error level determination generated by

$$\begin{aligned} &If\ u_c > h\ then\ u = +1 \\ &elseif\ u_c < -h\ then\ u = -1 \end{aligned} \tag{12}$$

where *h* shows the error level and has very small value. A more detail on converter control is given in [22].

5.2. VSC structure of other DGs

The VSC structure of all the other micro sources are the same as the structure of the compensator but there is an inductance at their output connection point for controlling the amount of active and reactive power injected to the network. The same controlling method in the previous section is being used for generating the switching pulses of the IGBTs in these converters, too.

6. MODELLING OF MICROGRID

As described in Section 2, there are four DGs in the microgrid. The diesel genset is modeled as in [23] and is not discussed in the paper. Other three DG models and associated power electronic controllers are discussed below and their technical data are given in Appendix B.

6.1. Fuel Cell (FC)

FCs are emerging as an attractive power supply source for applications such as distributed generation because of their cleanness, high efficiency, and high reliability. A review on the FC technology, characteristics and research area is given in [24]. Usually four types of FCs, named PEMFC, PAFC, MCFC and SOFC, classified based on their electrolyte type, are used in electrical utilities for electric power generation [25]. A mathematical model for investigating the dynamic performance of a PEMFC was developed in [26]; this model is based on physical laws having clear significance in replicating the FC system and can easily be used to set up different operational strategies. From the empirical point of view, [27] formulated a model that enables simulation of the V-I curve of FCs in typical conditions. Different from the normal PEMFC model, a purely electronic circuit model similar to characteristics of a PEMFC was introduced in [28] that can be used to design and analyze FC power systems using electric circuit elements. As an experiment, the steady-state performance and transient response for hydrogen and oxygen flow in PEMFCs is investigated in [29].

In this paper, a typical PEMFC with simplified model of Fig. 5 and output V-I characteristic of (13), verified experimentally and reported in [30] is used. Similar characteristic is given for all FCs in [26-28] where their numerical values differ according to their rating, output voltage and application. The studies in this paper are based on the output electric power point of view and physical-chemical characteristics of FCs such as hydrogen and oxygen pressure are not investigated. The V-I characteristic of the FC is given by

$$V(i) = 371.3 - 12.38\log(i) - 0.2195i - 0.2242e^{0.025i} \tag{13}$$

A boost chopper is used at FC output for regulating the necessary DC voltage v_c across the capacitor. The schematic diagram of the simulated FC model with the output chopper is shown in Fig. 5.

FCs have several shortcomings [28] such as no energy storage possibility, slow dynamic response, output voltage fluctuation with load and difficult cold start. Therefore, an electric storage such as battery or ultracapacitor must be accompanied with FC to improve its dynamic characteristics. If the storage is in parallel directly with the DC bus, its charge and discharge cannot be controlled [28]; therefore, a bidirectional converter is needed between the DC bus and the electric storage to control its state of charge. A detailed control basics and algorithm for the bidirectional converter of the storage is presented and verified in [31]. The studies carried out in the paper, show that the FC has a good and acceptable dynamic response for power quality improvement and power sharing objectives and no storage unit on FC was used in this paper.

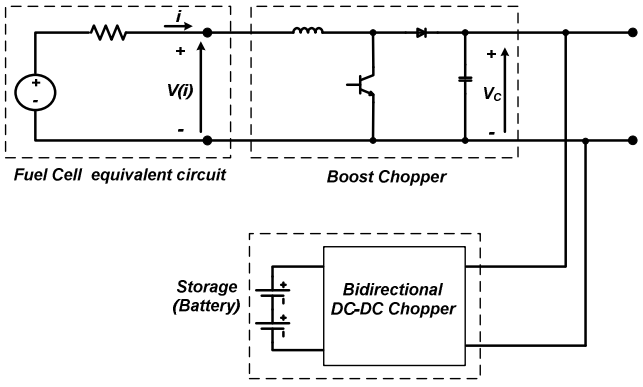

Fig. 5. Fuel cell and storage modeled equivalent circuit.

6.2. Photovoltaic Cell (PV)

A series and parallel combination of PV cells constitute a PV array. Fig. 6 shows the simplified equivalent circuit where output voltage is a function of the output current while the current is a function of load current, ambient temperature and radiation level [32]. The voltage equation of the PV is calculated by

$$V_{PV} = \frac{AkT_c}{e} Ln\left(\frac{I_{ph} + I_o - I_c}{I_o}\right) - R_s I_c \tag{14}$$

where

A: constant value for curve fitting
e: electron charge (1.602×10-19 C)
k: Boltzmann constant (1.38×10-23 J/^{o}k)
I_c: output current of PV cell
I_{ph}: photocurrent (1 A)
I_o: diode reverse saturation current (0.2 mA)
R_s: series resistance of PV cell (1 mΩ)
V_{PV}: output voltage of PV cell
T_c: PV cell reference temperature (25^{o}C)

The output chopper controls the voltage v_c across the capacitor. A Maximum Power Tracking (MPPT) method is used to set the reference voltage of the chopper to achieve maximum power from the PV based on the load or ambient condition changes. The MPPT algorithm used in this paper is given in [32]. A PI controller is used in the chopper in order to achieve the desired reference voltage set by the MPPT. A battery storage system is connected in parallel with the DC bus of the chopper output through a bidirectional converter which is used to control the charging and discharging the battery. Depending on the terminal voltage of the PV, the battery gets charged or discharged. A more detailed explanation on bidirectional converter control of PV storage system is given in [33].

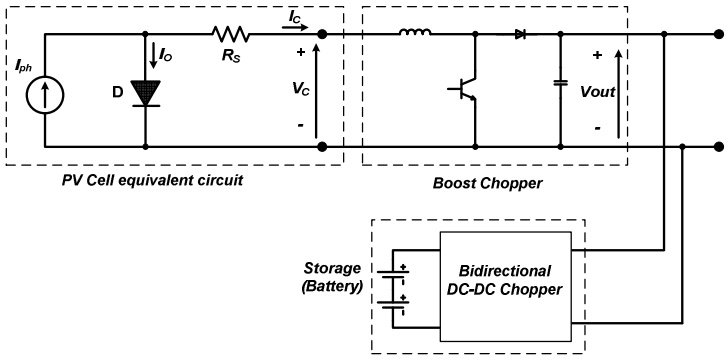

Fig. 6. Equivalent circuit of PV, boost chopper based on MPPT and storage.

6.3. Battery

The battery is assumed to be a constant voltage source with fixed amount of energy and modeled as a constant DC voltage source with series internal resistance where the VSC is connected to its output. The battery has a limitation on the duration of its generated power and depends on the amount of current supplied by it. It is assumed that the battery is charged at the off-peak load periods of the network and is discharged at peak load times through the converter.

7. STUDY CASE AND SIMULATION RESULTS

The system is simulated in various operating conditions with different load demand in the microgrid. The simulation results are discussed below.

7.1. Case 1- Compensator principle operation

In this case, the simple structure of Fig. 2 is simulated to investigate the compensator effects on power quality improvement of the load. An unbalanced and harmonic load which causes a 9.3% and 1.47% unbalance in the network current and voltage respectively is connected to an ideal voltage source. In addition to that, the nonlinear load has a 9.8% and 8.2% THD in the current and voltage respectively. The compensator is connected to the network at 0.05 sec. In Fig. 7, the network voltage (V_P) and current driven from the source (I_{MG}) are shown before and after the compensation. As shown in this figure, the compensator is injecting the necessary current to PCC to balance the voltage and therefore, the current drawn from the source

is forced to be balanced. In Fig. 8, the initial and final values of the unbalance and THD of network current and voltage are shown before and after the compensator connection. The current and voltage unbalance values are limited to less than 0.2% and 0.05% respectively while the same values for THD are respectively less than 0.4% and 0.2%. Fig. 9 illustrates the FFT diagrams and proves the reduction of the harmonic orders of network current and voltage after compensator connection compared to the harmonic order values before the compensation.

The proposed compensator is also capable of complete reactive power compensation and power factor correction by injecting the exact amount of the reactive power demand of the nonlinear load. In Fig. 10, the instantaneous voltage and current waveforms are shown together where the phase difference is obvious before the compensator connection which is minimized to zero after the compensation and the power factor is corrected to unity.

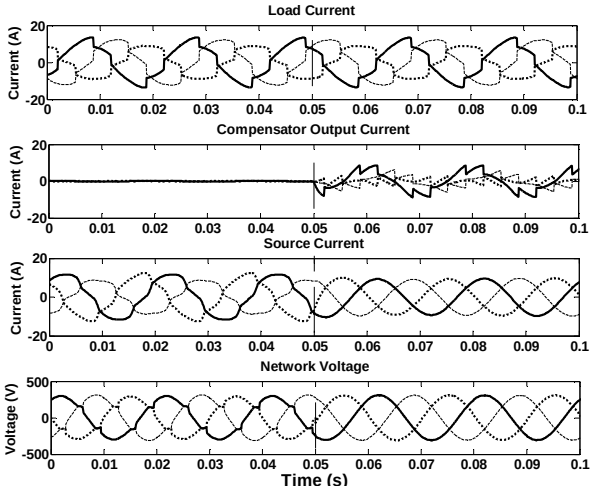

Fig. 7. Load current, compensator output current, source current and network voltage before and after compensation.

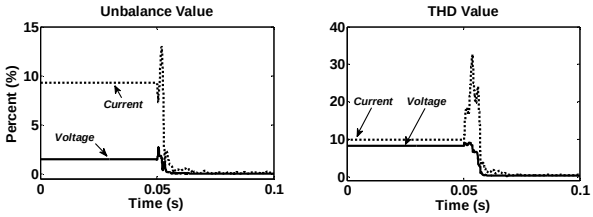

Fig. 8. Unbalance and THD values of network current and voltage before and after compensation.

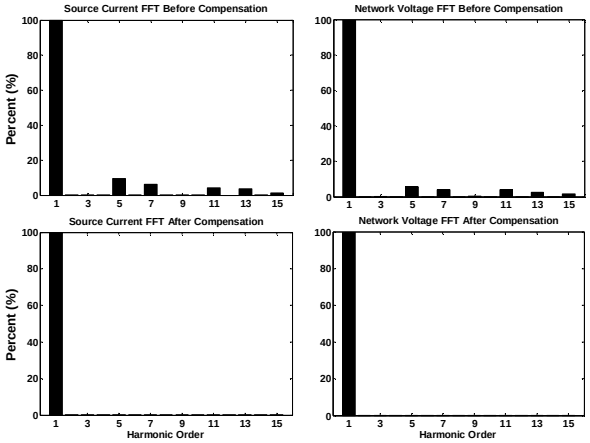

Fig. 9. FFT spectrum of network current and voltage before and after compensation.

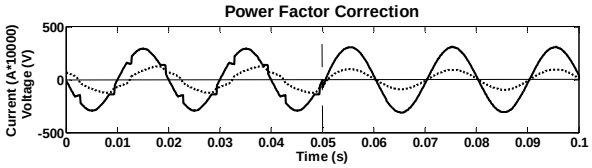

Fig. 10. Power factor correction.

7.2. Case2- Power sharing in microgrid

In this case, the microgrid operation has been investigated during autonomous mode. In autonomous mode, total power demand is shared among the DGs proportional to their rating. For investigating the dynamic response of the controller, two incidents, including load change and power limiting of a DG are studied in the microgrid structure of Fig. 1. In this case, it is given that the nonlinear load is not connected to the network and therefore, FC is just working like other micro sources in power sharing. It is assumed that the system is operating in steady state while all the micro sources are connected and supplying all the loads except the 6 kW fan heater load. At 0.4 sec., there is a sudden power limitation on the output power of the PV which is reduced from 2.43 kW to 1 kW. Therefore, the other DG units are responsible for supplying the rest of the required power to the loads. Hence, the output power of the other DG units is increased but still with respect to their rated power. The second incident that occurs is the connection of the 6 kW fan heater load to the network at 0.9 sec. Increase of power demand in the network results in the output power increase of the DG units with respect to their rated values except the PV which is still working in power limit mode. The power response of the DGs and controller in the microgrid are shown in Fig. 11 and the numerical values of the power sharing in this case are given in Table 1. The dynamic of the step response of the network proves that the microgrid system and controller stabilizes to steady state condition within 5-6 cycles.

The power dispatch among the PV cell and its storage is shown in Fig. 12. In this figure, it is assumed that PV cell was generating 2.6 kW which (minus the inverter loss) is feeding into the microgrid. At 0.5 sec., the PV active power generation has increased to 6.4 kW. Therefore, the surplus energy (3.75 kW) is saved into the storage unit. At 1 sec., it is assumed that there is a limitation on the PV power generation but since the storage unit is already charged, the required power is fed into microgrid by the storage. If at 1.5 sec. the PV is again able to produce the required power and hence output power of storage returns to zero.

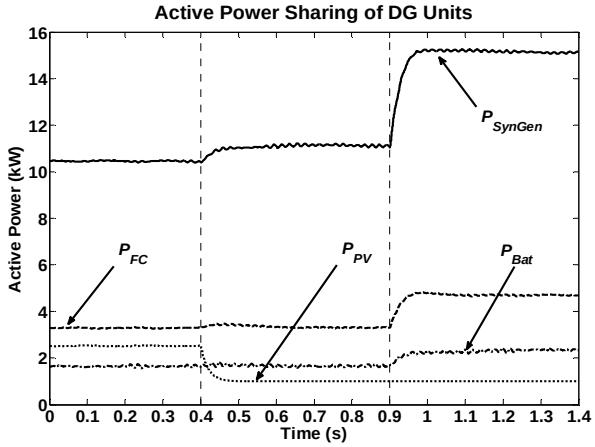

Fig. 11. Active power sharing of DGs in microgrid in autonomous mode for load change and PV power limiting.

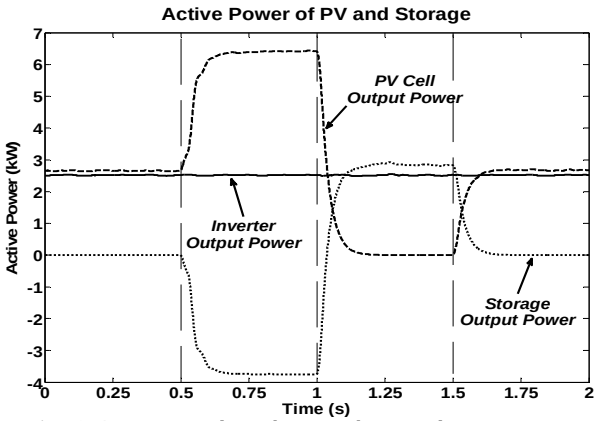

Fig. 12. Active power dispatch among the PV and its storage unit.

Table 1
Numerical values of power sharing of the micro sources in microgrid [kW]

	P_{SynGen}	P_{FC}	P_{Bat}	P_{PV}
steady state	10.46	3.28	1.64	2.51
power limiting in PV	11.1	3.29	1.68	1
load change	15.1	4.67	2.37	1

7.3. Case 3- Microgrid with nonlinear load

In this case, the FC converter is controlled not only to supply power to the microgrid but also to improve the power quality of the network. The nonlinear load is connected to BUS 5 where the FC is connected and circuit breaker CB_1 is open. The nonlinear load is a combination of unbalanced and harmonic load of Case 1. Depending on the nonlinear load power demand, the compensator can work in Mode I or Mode II. It is assumed that the microgrid is operating in steady state while the compensator is operating in Mode I. In this mode, the FC is supplying the whole power demand of the nonlinear load and the rest of its rated power is fed to the microgrid as discussed in Section 4. At 0.25 sec., the power demand of the nonlinear load is increased to more than the rated power of the FC. Therefore, the operation mode of the converter is changed to Mode II and it is desired that the FC supplies half of the power demand of the nonlinear load ($\lambda_P = \lambda_Q = 0.5$) while the other half is supplied by the microgrid. At 1.25 sec., the power demand of the nonlinear load is decreased to the initial value and the compensator is returned back to Mode I. The power output of the compensator (FC), power from the microgrid to PCC and the power demand of the nonlinear load are shown together in Fig. 13. The active power sharing among other micro sources according to the operation mode of the compensating DG is also shown in Fig. 14. The numerical results of the active power of all the DG units, nonlinear load and power from microgrid to PCC are given in Table 2. The RMS voltage of the network, variation of which is kept in a limit of ± 5%, increase and decrease due to the changes in the nonlinear load power demand, as shown in Fig. 15.

In the same case, for investigating the effects of compensator on the voltage and current conditions of the network, the waveforms at PCC are shown separately in the absence and presence of the compensator in Fig. 16. By comparing the waveforms, it is obvious that the compensator has been able to effectively improve the unbalance and THD values. The numerical values of unbalance and THD of current and voltage of the microgrid at PCC with and without compensator are given in Table 3.

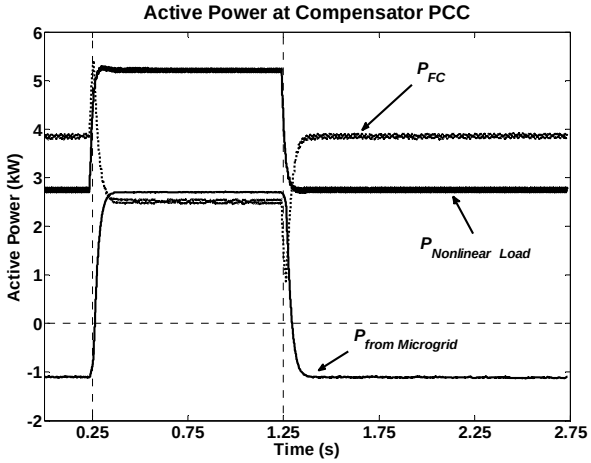

Fig. 13. Active power output of compensator (FC), power from the microgrid to PCC and the power demand of the nonlinear load.

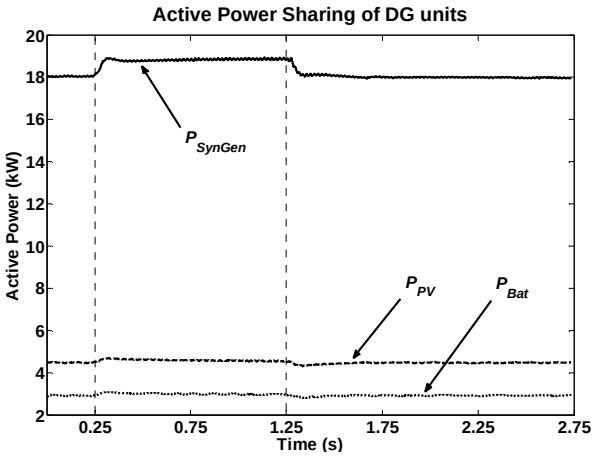

Fig. 14. Active power sharing of synchronous generator, PV and battery during Mode I and II operating conditions of the compensator.

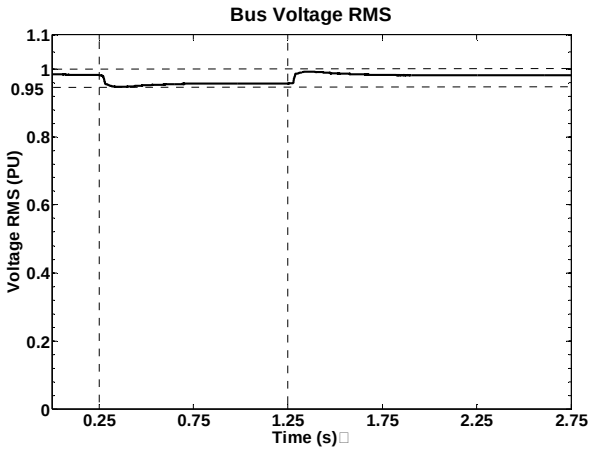

Fig. 15. Microgrid voltage RMS variations.

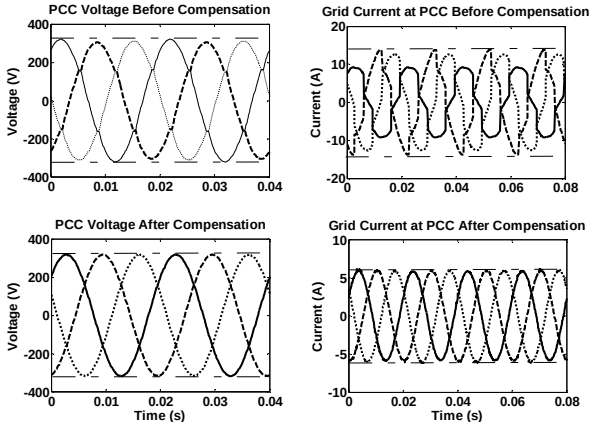

Fig. 16. PCC voltage and current instantaneous waveforms of microgrid with and without compensator.

Table 2
Numerical values of active power sharing of the DGs [kW] and the error with the expected values [%]

	P_{SynGen}	$P_{PV\ (error)}$	$P_{Bat\ (error)}$	P_{NL}	$P_{comp.\ (FC)}$	P_{MG}
with compensator (Mode I)	17.99	4.46 (1%)	2.91 (3%)	2.78	3.88	-1.1
with compensator (Mode II)	18.92	4.52 (4%)	2.93 (5%)	5.17	2.47	2.7
without compensator	19.47	4.82 (1%)	3.14 (3%)	4.88	0	4.88

Table 3
Numerical values of THD and unbalance of current and voltage before and after compensation [%]

	THD		Unbalance	
	Before compensation	After compensation	Before compensation	After compensation
I_{MG}	12.7	< 1.5	10.5	< 2
V_P	3.3	< 0.5	0.7	< 0.2

7.4. Case 4- Microgrid supplying single-phase residential loads

Each residential load is usually supplied form one phase of a three-phase system. In addition, any residential customer can have a rooftop PV system, which is also single-phase in nature. These rooftop PVs can have different ratings and they can export power to the microgrid. Therefore, not only the nature of the single-phase loads can increase the unbalance in the current in the network, but also the active power amount and direction can change. Therefore, such residential supply such grid connected PV systems can have much worse effect on the unbalance characteristics of the network.

For this study, the nonlinear load of case 3 has been replaced with a low voltage residential distribution network with the characteristics explained above. The schematic diagram of this network is shown in Fig. 17 and its technical data is given in Appendix B. For this study, it is assumed that the microgrid with distribution network is in its steady state where at 0.5 sec. the compensator is connected to the network and starts functioning in Mode I. The compensator connection also improves the voltage profile of the network and removes the voltage sag effect due to high power demand of the loads. It is assumed that at 1.5 sec. a load change is applied in the distribution network which causes the compensator to start operating in Mode II. The active power sharing of micro sources (genset, PV and battery), active power dispatch at PCC (including power generated by compensator, power from microgrid to PCC and power demand of residential distribution network) and also the power dispatch at each phase of the residential distribution network are shown separately in Fig. 18. The variation of the voltage RMS of the network is also shown in Fig. 19 which is kept in the acceptable range of 5%. Figures 20 and 21 respectively show the voltage and current instantaneous and unbalance values at 0.5 sec. where the compensator is connected to the network. From these results, the efficacy of the proposed controller for power quality improvement is evident.

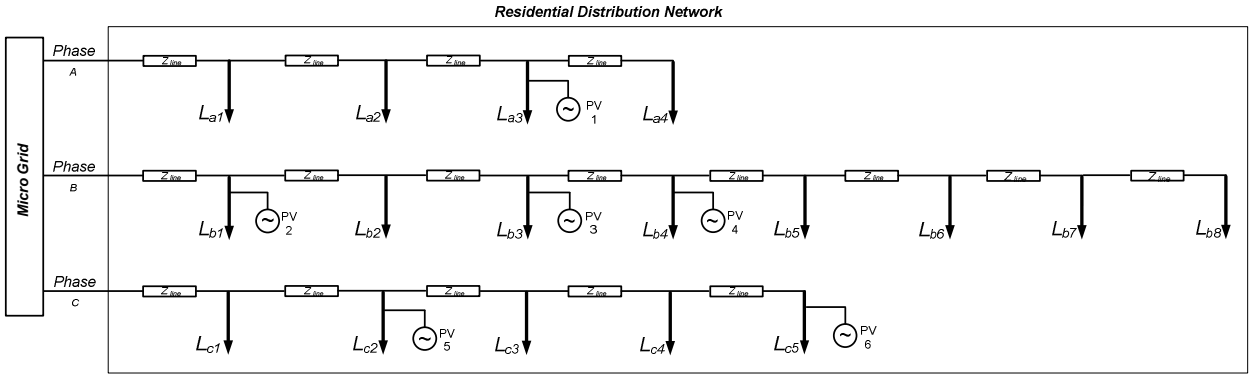

Fig. 17. Schematic diagram of the low voltage residential distribution network.

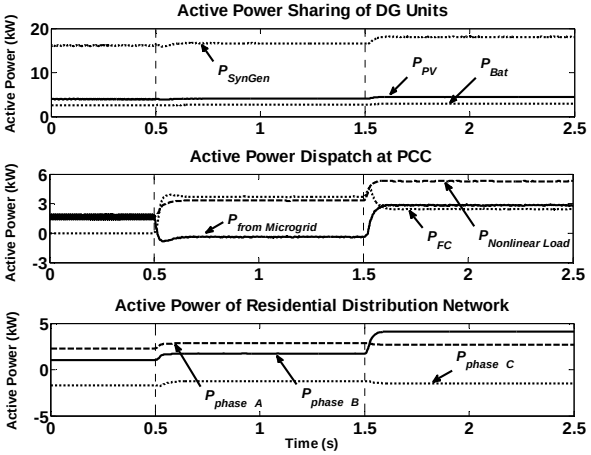

Fig. 18. Active power sharing of DG units, Active power dispatch at PCC, Active power dispatch at each phase of the residential distribution network.

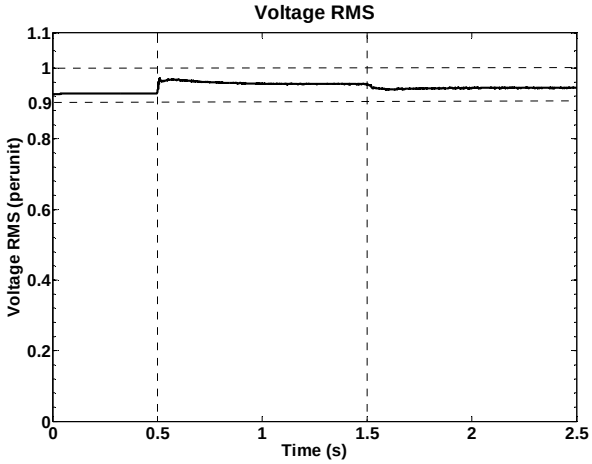

Fig. 19. Microgrid voltage RMS variations.

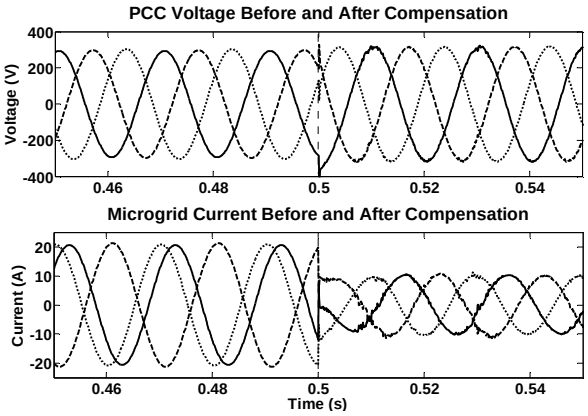

Fig. 20. PCC voltage and current instantaneous waveforms of microgrid with and without compensator.

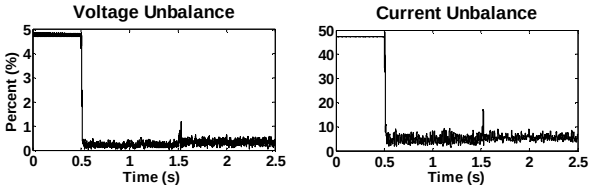

Fig. 21. Unbalance values of PCC current and voltage in microgrid before and after compensation.

8. CONCLUSION

The power quality improvement in a hybrid microgrid has been discussed in this paper. The hybrid microgrid consisted of inertial and converter interfaced micro sources where a decentralized power sharing algorithm based on droop control is used. One DG, used as compensator, is able to compensate the nonlinear (unbalanced and harmonic load) of the microgrid while other DGs share the power. The proposed control scheme can change its mode of operation seamlessly depending on the power demand of the nonlinear load. The extension of the nonlinear load to a low voltage residential distribution network shows the possibility of supplying single-phase residential loads with some PVs. Inclusion of the micro source model ensures proposed power electronic control can work in tandem with the associated dynamics of micro sources. A stable operation in various operating condition shows the efficacy of proposed control scheme.

ACKNOWLEGEMENT

This work was supported by Australian Research Council for the financial support for this project through ARC Discovery Grant DP 0774092.

APPENDIX A- EFFECT OF COMPENSATING DG LOCATION

Let us consider a three-phase distribution system with structure shown in Fig. 22 where a nonlinear load is connected to BUS 6. BUS 1 is assumed to be stiff and the feeders have impedance. The implications of placing the compensator at various buses of this figure are listed in Table I. It is evident from the table that the compensator can make the voltages of all the buses sinusoidal if it is connected at the same bus in which the nonlinear load is connected [22].

In Fig. 23, the voltage waveforms of BUS 1 and PV output current are shown when the nonlinear load is connected to BUS 1 of microgrid structure of Fig. 1. It can be seen that both voltage and current are unbalanced and the distortion in the voltage waveform is obvious. Similar waveforms can be shown for all other buses except BUS 5 at which the compensator is connected.

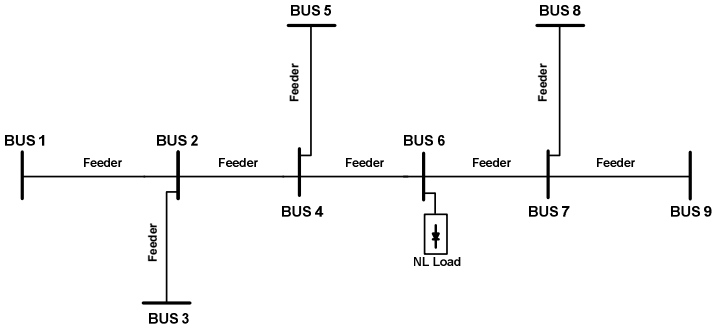

Fig. 22. A schematic single line diagram of a microgrid.

Table I
Effected buses due to implication of compensator in various buses

Compensator at bus	Voltage distortion at buses	Sinusoidal voltage at buses
BUS 2	BUS 4 to 9	BUS 2 to 3
BUS 3	BUS 2, 4 to 9	BUS 3
BUS 4	BUS 6 to 9	BUS 2 to 5
BUS 5	BUS 2 to 4, 6 to 9	BUS 5
BUS 6	None	All
BUS 7	BUS 2 to 6	BUS 7 to 9
BUS 8	BUS 2 to 7, 9	BUS 8
BUS 9	BUS 2 to 8	BUS 9

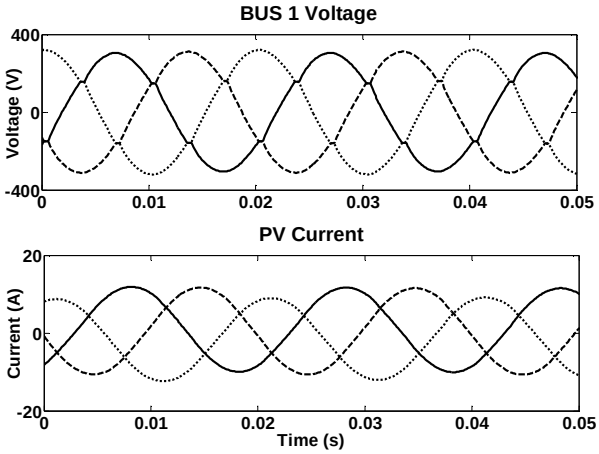

Fig. 23. BUS1 Voltage and PV current waveforms when the nonlinear load is connected to BUS 1 of microgrid.

APPENDIX B- TECHNICAL DATA AND PARAMETERS

Table II
Grid and Load Types in the Microgrid

Grid	
Voltage	415 V L-L RMS
Frequency	50 Hz
Line Impedance	R =0.02 Ω, L =0.001 H
Load Type	
Fan Heater	3 three-phase Resistive Load each P =4.5 kW
Fan Heater	1 three-phase Resistive Load P =6 kW
Induction Motor	6 three-phase each P =1.5 kW

Table III
PV, Boost Chopper, Converter and Controller

No. of PV cells in series	2
No. of PV cells in parallel	3
Output voltage of PV cell	0.1 V DC
Rated output power	3.06 kW
Radiation level	1100
Ambient Temperature	30 ^{oC}
Output voltage of Chopper	250 V DC
Boost Chopper Parameters	L =10 mH, C = 5 mF
Boost Chopper Controller	Hysteresis Voltage Control, k_p =0.0001, Hys.$_{bandwidth}$ =0.0002
Converter Structure	3 Single-Phase H-Bridge Inverter
Converter Loss	R =0.1 Ω per phase
Transformer	0.25/0.415 kV, 0.5 MVA, Lr=4.4 mH
LC Filter	L_f=49.8 mH, C_f=50 µF
Hysteresis Constant	10^{-5}

Table IV
Battery, Converter and Controller

No. of battery units in series	10
No. of battery units in parallel	2
output voltage of battery unit	12 V DC
Rated output power	2 kW, 226 A.hr
Converter Structure	3 Single-Phase H-Bridge Inverter
Converter Loss	R=0.1 Ω per phase
Transformer	0.12/0.415 kV, 0.5 MVA, Lr=4.4 mH
LC Filter	L_f=76.2 mH, C_f=50 µF
Hysteresis Constant	10^{-5}

Table V
Fuel Cell, Boost Chopper, Converter and Controller

Fuel cell rated power	4 kW
Boost Chopper Parameters	L =1 mH, C =1 mF, f_{sw} =10 kHz
Boost Chopper Controller	Open loop control, Switch duty cycle=10%
Converter Structure	3 Single-Phase H-Bridge Inverter
Converter Loss	R =1.5 Ω per phase
Transformer	0.4/0.415 kV, 0.25 MVA, Lr=0.54 mH
LC Filter	L_f=38.1 mH, C_f=50 µF
Hysteresis Constant	10^{-5}

Table VI
Diesel Generator Set

Structure	Internal Combustion Engine + Exciter + 3 phase Synchronous Generator
Rated power	14 kVA
Rated voltage	415 V L-L RMS
Rated Frequency	50 Hz, 1500 rpm

Table VII
Droop Controller Coefficients

DG Type	$m_{Active\ Power\text{-}Angle}$ **[rad/MW]**	$n_{Reactive\ Power\text{-}Voltage}$ **[kV/Mvar]**
PV	441	0.196
FC	337.5	0.15
Battery	675	0.30
Syn. Generator	112.5	0.05

Table VIII
Residential Low voltage Distribution Network

Grid	
Voltage	415 V L-L RMS
Frequency	50 Hz
Line Impedance	R =0.02 Ω, L =0.001 H (between each load)

Loads (values at the time of simulation)

L_{a1}= *1.9 kW*	L_{a2}= *2.3 kW*	L_{a3}= *2.3 kW*	L_{a4}= *2.3 kW*	L_{b1}= *2.4 kW*	L_{b2}= *3.8 kW*
L_{b3}=*2.5 kW*	L_{b4}= *2.2 kW*	L_{b5}= *1.7 kW*	L_{b6}= *1.9 kW*	L_{b7}= *2.3 kW*	L_{b8}= *2.3 kW*
L_{c1}= *1.9 kW*	L_{c2}= *2.8 kW*	L_{c3}= *2.2 kW*	L_{c4}= *2.3 kW*	L_{c5}= *2.5 kW*	

Single-Phase PVs

PV_1=*1 kW*	PV_2=*2 kW*	PV_3=*1 kW*
PV_4=*1 kW*	PV_5=*3 kW*	PV_6=*3 kW*

REFERENCES

[1] G. Pepermans, J. Driesen, D. haeseldonckx, R. Belmans, W. D'haeseleer, Distributed generation: definition, benefits and issues, Energy Policy, Vol. 33, pp. 787-798, 2005.

[2] D. Menniti, C. Picardi, A. Pinnarelli, D. Sgro, Power management by grid connected inverters using a voltage and current control strategy for microgrid applications, in Proc. of Int. Symp. on Power Electronics, Electrical Drives, Automation and Motion (SPEEDAM), pp. 1414-1419, 2008.

[3] A. Tuladhar, H. Jin, T. Unger, K. Mauch, Parallel operation of single phase inverter modules with no control interconnections, IEEE 12th Annual Applied Power Electronics Conf. (APEC), Vol. 1, pp. 94-100, Feb. 1997

[4] V. Calderaro, J.V. Milanovic, M. Kayikci, A. Piccolo, The impact of distributed synchronous generators on quality of electricity supply and transient stability of real distribution network, Electric Power Systems Research, Vol. 79, pp. 134-143, 2009.

[5] K.H. Chao, S.H. Ho, M.H. Wang, Modeling and fault diagnosis of a photovoltaic system, Electric Power Systems Research, Vol. 78, Issue 1, pp. 97-105, Jan. 2008.

[6] T. kaipia, P. Peltoniemi, J. Lassila, P. Salonen, J. Partanen, Power electronics in smart grids-impact on power system reliability, in Proc. of CIRED Int. Conf., Germany, June 2008.

[7] J.M. Guerrero, L.G. de Vicuna, J. Matas, M. Castilla, J. Miret, A wireless controller to enhance dynamic performance of parallel inverters in distributed generation systems, IEEE Trans. on Power Electronics, Vol. 19, No. 5, pp. 1205-1213, 2004.

[8] M.C. Chandorkar, D. M. Divan, R. Adapa, Control of parallel connected inverters in standalone AC supply systems, IEEE Trans. on Industry Applications, Vol. 29, No. 1, pp. 136-143, 1993.

[9] R.T. Jagaduri, G. Radman, Modeling and control of distributed generation systems including PEM fuel cell and gas turbine, Electric Power Systems Research, Vol. 77, Issue 1, pp. 83-92, Jan. 2007.

[10] R. Lasseter, Microgrids, in Proc. of IEEE 2002 Power Engineering Society Winter Meeting, 2002.

[11] N. Hatziargyriou, H. Asano, R. Iravani, C. Marnay, Microgrids, IEEE Power and Energy Magazine, Vol. 5, No. 4, pp. 78-94, July-August 2007.

[12] F. Katiraei, M. Iravani, Power management strategies for a microgrid with multiple distributed generation units, IEEE Trans. on Power Systems, Vol. 21, No.4, pp. 1821-1831, Nov. 2006.

[13] J. A. Peças. Lopes, C. L. Moreira, A. G. Madureira, Defining control strategies for microgrids islanded operation, IEEE Trans. on Power Systems, Vol. 21, No. 2, pp. 916-924, May 2006.

[14] F. Katiraei, M. Iravani, P. W. Lehn, Microgrid autonomous operation during and subsequent to islanding process, IEEE Trans. on Power Delivery, Vol. 20, No.1, pp. 248-257, Jan. 2005.

[15] C. L. Moreira, F. O. Resende, J. A. Peças Lopes, Using low voltage microgrids for service restoration, IEEE Trans. on Power Systems, Vol. 22, No. 1, pp. 395-403, Feb. 2007.

[16] P. Piagi, R. Lasseter, Autonomous control of microgrids, in Proc. of IEEE 2006 Power Engineering Society General Meeting, 2006.

[17] N. L. Soultanis, S. A. Papathanasiou, N. Hatziargyriou, A stability algorithm for the dynamic analysis of inverter dominated unbalanced LV microgrids, IEEE Trans. on Power Systems, Vol. 22, No. 1, pp. 294-304, Feb. 2007.

[18] R. Lasseter, P. Piagi, Providing premium power through distributed resources, in Proc. of IEEE 33rd Hawaii Int. Conf. on System Sciences, 2000.

[19] R. C. Dugan, M. F. McGranaghan, S. Santoso, H. W. Beaty, Electrical Power Systems Quality, 2nd Ed., McGraw-Hill, New York, 2002.

[20] Y. Li, D. M. Vilathgamuwa, P. C. Loh, Microgrid power quality enhancement using a three phase four wire grid interfacing compensator, IEEE Trans. on Industry Applications, Vol. 41, No. 6, pp. 1707-1719, 2005.

[21] R. Majumder, A. Ghosh, G. Ledwich, F. Zare, Load sharing and power quality enhanced operation of a distributed microgrid, IET Renewable Power Generation, Vol. 3, Issue 2, pp. 109-119, June 2009.

[22] A. Ghosh, G. Ledwich, Power quality enhancement using custom power devices, Kluwer Academic Publishers, 2002, ISBN: 1402071809.

[23] S. Krishnamurthy, T.M. Jahns, R.H. Lasseter, The operation of diesel gensets in a CERTS microgrid, IEEE Power and Energy Society General Meeting- Conversion and Delivery of Electrical Energy in 21st Century, pp. 1-8, July 2008.

[24] P. Sethakul, S. Rael, B. Davat, P. Thounthong, Fuel cell high-power applications, IEEE Industrial Electronics Magazine, Vol. 3, No. 1, pp. 32-46, March 2009.

[25] B. Viswanathan, M. Aulice Scibioh, Fuel Cells Principles and Applications, CRC Press LLC, 2007, ISBN: 1420060287.

[26] S. Yerramalla, A. Davari, A. Feliachi, T. Biswas, Modelling and simulation of the dynamic behavior of a polymer electrolyte membrane fuel cell, Journal of Power Sources, Vol. 124, No. 1, pp. 104-113, Oct. 2003.

[27] S. Busquet, C. E. Hubert, J. Labbe, D. Mayer, R.Metkemeijer, A new approach to empirical electrical modeling of a fuel cell, an electrolyser or a regenerative fuel cell, Journal of Power Sources, Vol. 134, No. 1, pp. 41-48, July 2004.

[28] D. Yu, S. Yuvarajan, Electronic circuit model for proton exchange membrane fuel cells, Journal of Power Sources, Vol. 142, No. 1/2, pp. 238–242, March 2005.

[29] Q. Yan, H. Toghiani, H. Causey, Steady state and dynamic performance of proton exchange membrane fuel cells (PEMFCs) under various operating conditions and load changes, Journal of Power Sources, Vol. 161, No. 1, pp. 492-502, Oct. 2006.
[30] Y. Hou, G. Wan, W. Jiang, M. Zhuang, Steady state performance modeling of a fuel cell engine, IEEE Int. Conf. on Vehicular Electronics and Safety (ICVES), pp. 424-427, Dec. 2006.
[31] K. Jin, X. Ruan, M. Yang, M.xu, Power management for fuel-cell power system cold start, IEEE Trans. on Power Electronics, Vol. 24, No. 10, pp. 2391-2395, Oct. 2009.
[32] I.H. Altas, A.M. Sharaf, A novel photovoltaic on-line Search algorithm for maximum energy utilization, in proc. of Int. Conf. on Communication, Computer and Power (ICCCP), Oman, Feb. 2007.
[33] R. Gules, J.D.P. Pacheco, H.L. Hey, J. Imhoff, A maximum power point tracking system with parallel connection for PV stand-alone applications, IEEE Trans. on Industrial Electronics, Vol. 55, No. 7, pp. 2674-2683, July 2008.